GEOPHYSICS, VOL. 74, NO. 2 (MARCH-APRIL 2009); P. WA123–WA135, 12 FIGS., 1 TABLE.
10.1190/1.3043726

The robustness of seismic attenuation measurements using fixed- and variable-window time-frequency transforms

Carl Reine[1], Mirko van der Baan[1], and Roger Clark[1]

ABSTRACT

Frequency-based methods for measuring seismic attenuation are used commonly in exploration geophysics. To measure the spectrum of a nonstationary seismic signal, different methods are available, including transforms with time windows that are either fixed or systematically varying with the frequency being analyzed. We compare four time-frequency transforms and show that the choice of a fixed- or variable-window transform affects the robustness and accuracy of the resulting attenuation measurements. For fixed-window transforms, we use the short-time Fourier transform and Gabor transform. The S-transform and continuous wavelet transform are analyzed as the variable-length transforms. First we conduct a synthetic transmission experiment, and compare the frequency-dependent scattering attenuation to the theoretically predicted values. From this procedure, we find that variable-window transforms reduce the uncertainty and bias of the resulting attenuation estimate, specifically at the upper and lower ends of the signal bandwidth. Our second experiment measures attenuation from a zero-offset reflection synthetic using a linear regression of spectral ratios. Estimates for constant-Q attenuation obtained with the variable-window transforms depend less on the choice of regression bandwidth, resulting in a more precise attenuation estimate. These results are repeated in our analysis of surface seismic data, whereby we also find that the attenuation measurements made by variable-window transforms have a stronger match to their expected trend with offset. We conclude that time-frequency transforms with a systematically varying time window, such as the S-transform and continuous wavelet transform, allow for more robust estimates of seismic attenuation. Peaks and notches in the measured spectrum are reduced because the analyzed primary signal is better isolated from the coda, and because of high-frequency spectral smoothing implicit in the use of short-analysis windows.

INTRODUCTION

Seismic attenuation can be caused by intrinsic effects such as anelastic losses resulting from fluid movement (Dvorkin and Nur, 1993) and friction between grains or crack faces (Johnston et al., 1979). Similarly, losses can occur by processes that mimic intrinsic effects such as multiple scattering. Typically, the overall effect on the seismic signal is that higher frequencies are suppressed more rapidly than lower frequencies as the signal propagates over greater distances or through more attenuating media. This results in a loss of signal resolution.

Conversely, the additional information that attenuation imparts to the signal can be a useful tool for reservoir characterization. For example, attenuation is sensitive to changes in gas saturation in partially saturated media (Winkler and Nur, 1982), and in fractured media, the magnitude of attenuation change with azimuth has been shown to be a useful indicator of fracture direction (Clark et al., 2001; Maultzsch et al., 2007). Finally, once attenuation is measured, it is possible to mitigate the resolution loss by applying processes such as inverse-Q filtering (Wang, 2002) to aid with structural interpretations (Kaderali et al., 2007), amplitude-variation-with-offset (AVO) analysis (Luh, 1993). Attenuation is therefore a desirable parameter to estimate; however, effects on the seismic spectrum from interference of different seismic arrivals often make its accurate determination elusive.

Among the many methods available for measuring seismic attenuation, frequency-based methods are common in exploration geophysics because of their reliability and ease of use (Tonn, 1991). Spectral estimates are required for these methods, which often are obtained using the short-time Fourier transform (STFT) (Dasgupta

Manuscript received by the Editor 20 March 2008; revised manuscript received 18 July 2008; published online 11 March 2009.
[1]University of Leeds, School of Earth and Environment, Earth Sciences, Leeds, U. K. E-mail: c.reine@see.leeds.ac.uk; m.van-der-baan@see.leeds.ac.uk; r.clark@see.leeds.ac.uk.

and Clark, 1998; Hauge, 1981). Time-frequency transforms, such as the continuous wavelet transform (Chakraborty and Okaya, 1995; Rioul and Vetterli, 1991) and S-transform (Stockwell et al., 1996), are available also, and they are becoming more popular. The continuous wavelet transform has found success in spectral decomposition (Sinha et al., 2005), and one of its benefits is its well-localized time extent, particularly at high frequencies.

A few investigations have compared different time-frequency transforms for specific applications. In the context of temporal resolution, Castagna and Sun (2006) compare the performance of the STFT and wavelet transform with other spectral estimates. They accomplish this by creating synthetic data using interfering wavelets of different frequencies, and they conclude that a variant of matching pursuit decomposition (Mallat and Zhang, 1993) has the best temporal resolution for their experiment. In the context of attenuation, Tai et al. (2006) compare the STFT and wavelet transform for their abilities to produce attenuation estimates in the presence of Gaussian random noise. Their work uses the spectral ratio method applied to a source wavelet and an isolated and attenuated version. Other works show that non-Fourier transforms can be used for attenuation estimates (e.g., Li et al., 2006), yet a formal comparison of transform types still is required in this context, and the aim of this paper is to provide this comparison.

The use of simple synthetics does not establish conclusively the superiority of one transform over another for attenuation estimates. Part of the issue with calculating a spectrum is that the seismic response is more complicated than a sparse convolutional model. The spectrum of recorded data is influenced by scattering losses and interference from short-path multiples (O'Doherty and Anstey, 1971; Shapiro and Zien, 1993). By obtaining estimates of the spectrum that are less affected by this interference, more confident and stable attenuation estimates can be made.

To address the complications of measuring a seismic spectrum, an investigation is required that looks at the behavior of different transform types in the presence of multiple scattering from numerous reflection interfaces. Here, we demonstrate that there are significant differences between the spectral estimates from two broad categories of time-frequency transforms: those having time windows that are fixed, and those with windows that are systematically varying with the frequency being analyzed. In the category of fixed-time-window transforms, we consider the STFT with both Hamming and Gaussian window functions, the latter referred to as a Gabor transform (Carmona et al., 1998). For variable-time-window transforms, we use the S-transform, and the continuous wavelet transform with a Morlet wavelet (Daubechies, 1992).

A third class of transform, which we do not consider, deals with parametric methods including Burg autoregressive estimates and matching pursuit decomposition. These methods allow for signal decomposition with spectral elements whose size is flexible (Wang, 2007). Although this property is useful for compactly describing signals or identifying major signal components, it makes a direct comparison with convolutional methods difficult. Whereas the basis functions for the transforms that we consider remain constant, the elements of parametric methods change depending on the signal, and it is not possible to apply conclusions from testing these methods to the general case.

We introduce first the algebraic description of seismic wave attenuation, and then give an overview of the time-frequency transforms that we use. To test which transforms produce the most robust and least biased attenuation estimates, we conduct two synthetic experiments and an analysis of real-surface seismic data. First we compare estimated and theoretical attenuation profiles resulting from multiple scattering. For this purpose, we model a transmission vertical seismic profile (VSP) and use wave localization theory (Shapiro and Zien, 1993) to calculate the expected attenuation.

Next we estimate constant-Q effective attenuation from a zero-offset reflection synthetic, and investigate the distribution of estimates for different bandwidths used in the linear regression of a natural log spectral ratio versus frequency. We repeat this analysis on a common-midpoint (CMP) supergather, and go on to investigate how well the measurements agree with expected behavior. Finally, we discuss reasons for the different performances, and the adequacy of each transform type for robust attenuation measurements.

THEORY

Attenuation

The amplitude spectrum of a wave in a homogeneous attenuating medium is given by

$$S(f) = S_0(f)e^{-\alpha z}, \tag{1}$$

where S is the amplitude of frequency f after propagating distance z, S_0 is the initial spectral amplitude, and α is the attenuation coefficient (Aki and Richards, 2002). By rearranging equation 1, attenuation might be determined from the spectral estimates of an initial S_0 and propagated event S:

$$\ln\left(\frac{S(f)}{S_0(f)}\right) = -\alpha z. \tag{2}$$

Although there are many definitions relating α and the seismic quality factor Q (Toverud and Ursin, 2005), we use the definition given by Aki and Richards (2002):

$$\alpha = \frac{\pi f}{QV}, \tag{3}$$

where V is the phase velocity of the wave in the medium.

Specifically for the case of a frequency-independent Q, by expressing a combination of equations 2 and 3 in terms of traveltime t,

$$\ln\left(\frac{S(f)}{S_0(f)}\right) = -\frac{\pi t}{Q}f, \tag{4}$$

a linear regression with frequency might be used to find the effective $1/Q_e$ for the medium. The effective value, however, is not controlled just by intrinsic effects such as fluid flow, but is affected also by apparent attenuation effects such as multiple scattering. The effective $1/Q_e$ is related to intrinsic $(1/Q_i)$ and apparent $(1/Q_{sc})$ effects through the following relationship (Spencer et al., 1982):

$$\frac{1}{Q_e} = \frac{1}{Q_i} + \frac{1}{Q_{sc}}. \tag{5}$$

Time-frequency transforms

A variety of methods are available to determine the spectra used in the measurement of $1/Q$. For nonstationary data, time-frequency

transforms are useful, as they produce a spectral estimate centered at each time element of the data. In this respect, a 1D data trace is mapped into a 2D spectrogram, which has dimensions of time and frequency.

Perhaps the most recognized time-frequency transform is the STFT, in which the data trace s is gated by a sliding window function w, and the Fourier transform (Bracewell, 1978) is applied to the result:

$$S_F(\tau,f) = \int_{-\infty}^{\infty} w(t-\tau)s(t)e^{-i2\pi ft}dt, \quad (6)$$

where τ is the time lag to the center of the window function. This definition allows for an arbitrary window function; however, by using a Gaussian window function,

$$w(t) = e^{-t^2/2\sigma^2}, \quad (7)$$

where σ is the distribution width, equation 6 takes on the definition of a Gabor transform (Carmona et al., 1998). This is because equation 6 becomes a convolution of the signal with a modulated Gaussian function, which is the impulse response of a Gabor filter (Rioul and Vetterli, 1991).

For our STFT analysis, we use a Hamming function (Harris, 1978), and for the Gabor transform, we use a fractional distribution width of $\sigma = 0.33$. The time length of the windows is set at 101 ms for the following analysis. This is suitable for measuring frequencies above 10 Hz, which have a period smaller than the window size. For data with lower frequency content, a larger window must be used.

The window functions chosen for the STFT and Gabor transform have a fixed time length for each frequency that is analyzed. Conversely, the S-transform (Stockwell et al., 1996) analyzes shorter data segments as the frequencies increase. This is accomplished by using the Gaussian window function (equation 7), and substituting a frequency-dependent expression for the distribution width:

$$\sigma = \frac{1}{|f|}. \quad (8)$$

Thus, by normalizing the window amplitude, the S-transform takes the form

$$S_S(\tau,f) = \frac{|f|}{\sqrt{2\pi}}\int_{-\infty}^{\infty} s(t)e^{-(t-\tau)^2f^2/2}e^{-i2\pi ft}dt. \quad (9)$$

Whereas the above transforms use the $e^{-i2\pi ft}$ basis function, the continuous wavelet transform uses scaled versions of a "mother wavelet" Ψ as its basis (Daubechies, 1992). This results in a transform of the form

$$S_W(\tau,a) = \frac{1}{\sqrt{a}}\int_{-\infty}^{\infty} s(t)\Psi^*\left(\frac{t-\tau}{a}\right)dt, \quad (10)$$

where a is the scale of the wavelet (Chakraborty and Okaya, 1995; Rioul and Vetterli, 1991). Although no explicit window function is used, the basis function itself has a restricted time extent, and therefore the time windowing is implicit in the choice of wavelet. Many mother wavelets exist, and as commonly done in seismic applications, we use a modulated Gaussian, or Morlet, wavelet. This is defined by Daubechies (1992) as

$$\Psi(t) = \pi^{-1/4}e^{-t^2/2}(e^{-i\omega_0 t} - e^{-\omega_0^2/2}), \quad (11)$$

with the constant ω_0 defined by

$$\omega_0 = \pi\sqrt{\frac{2}{\ln(2)}}. \quad (12)$$

After creating a high-frequency mother wavelet, the scale a is increased from its initial value. Thus, a time-scale decomposition is obtained, where increasing scale a corresponds to decreasing frequency f. For comparison with other time-frequency transforms, each scale must be mapped to the frequency that corresponds to the center frequency of the scaled wavelet. This is done by calculating the expression for the Nyquist frequency f_N in the oscillatory term in equation 11, and relating it to the initial frequency of the mother wavelet for discrete time with n points:

$$e^{-i\pi n} = e^{-i\omega_0 n}. \quad (13)$$

Therefore, the initial frequency of the mother wavelet is

$$f_0 = \frac{\omega_0}{\pi}f_N, \quad (14)$$

or

$$f_0 = \frac{\omega_0}{2\pi\Delta T}, \quad (15)$$

where ΔT is the sample rate of the data. The frequencies f of subsequent scales a then are found as a function of the initial frequency f_0 by

$$f = \frac{1}{a}f_0. \quad (16)$$

TRANSMISSION AND FREQUENCY-DEPENDENT ATTENUATION

Objective

The first test is a controlled experiment in which we compare estimated frequency-dependent attenuation with theoretically predicted profiles for a synthetic VSP. The purpose is to show that the type of transform used determines the precision and accuracy of the attenuation estimate. For this to be a meaningful test, two requirements must be met: (1) a geophysical model with known attenuation must be created, and (2) the seismic response of that model must be calculated to include all of the expected multiple reflections and interference. Although it is easy enough to design a finely layered model with known intrinsic attenuation, this does not account for the apparent attenuation caused by stratigraphic effects (O'Doherty and Anstey, 1971;

Schoenberger and Levin, 1974, 1978; Spencer et al., 1977). Conversely, a model with coarse layers might be created to isolate the intrinsic attenuation; however, this does not accurately represent realistic subsurface conditions.

Wave localization theory

To meet these conditions, we use wave localization theory, which describes the frequency-dependent attenuation of a transmitted wave caused by multiple scattering in a randomly layered medium (Shapiro and Zien, 1993). By generating an appropriate medium, we compare the estimated attenuation to the theoretical attenuation at each frequency, thereby evaluating the quality of the spectral estimate. Because wave localization theory involves a statistical description of the medium, it is possible then to create multiple model realizations and produce a statistical analysis of the attenuation estimates in terms of estimation variance and systematic error.

The random incompressibility fluctuations for a piecewise continuous medium display an exponential autocorrelation function,

$$\phi(\zeta) = \sigma_\kappa^2 e^{-|\zeta|/a_c}, \tag{17}$$

where ϕ is the autocorrelation function in terms of depth lag ζ, σ_κ is the relative standard deviation of the incompressibility fluctuations, and a_c is their characteristic scale length (van der Baan, 2001). For this type of medium, wave localization theory can be used to show that the theoretical apparent attenuation coefficient α is given by

$$\alpha = \frac{\sigma_\kappa^2 \pi^2 a_c f^2}{16 a_c^2 \pi^2 f^2 + V^2}, \tag{18}$$

where f is frequency and V is the average velocity (Shapiro and Zien, 1993; van der Baan, 2001).

This function shows how the energy of the primary arrival is scattered into a time-delayed sequence of arrivals referred to as the coda. Low frequencies, having larger wavelengths, see the random layering as an effective medium, and the amount of scattering is negligible. This results in apparent attenuation decreasing to zero in the low-frequency limit. The maximum scattering of energy occurs for frequencies with wavelengths that approach the typical scale a_c of the medium. Finally, as frequencies increase, the attenuation coefficient α decreases and converges to a constant value because the medium is piecewise continuous and smaller wavelengths are resolved for each layer (van der Baan, 2001).

Test setup

Using the procedure outlined by van der Baan et al. (2007), we analyze the sonic log of a well that penetrates a shallow sequence of alternating sands and shales. Assuming incompressibility fluctuations that observe an exponential autocorrelation function, and using a constant density, we then determine the parameters that describe the data. This is done by removing a polynomial trend from the velocity data, from which the zero-order term is used to give the mean velocity. Next the autocorrelation function is calculated. The zero-lag value of the autocorrelation, by equation 17, gives the value of σ_κ^2. Similarly, the characteristic scale is the depth lag where

$$\phi(a_c) = \sigma_\kappa^2 e^{-1}. \tag{19}$$

We then use these parameters to create a reasonable set of model properties for our medium, as well as three variants of this model (Table 1). Following the method described by van der Baan (2001), we generate 20 realizations of a random medium for each model, and from these produce VSP synthetics.

We consider the vertical transmission of a seismic wave through 500 m of the random medium, with an overlying 11-m homogeneous layer. An explosive source is placed at 10-m depth, and a receiver is placed at 510 m. The modeling is done using a reflectivity method, as implemented by Dietrich (1988), and to eliminate surface reflections, no free surface is used in the computation of synthetic waveforms. The source used is a 70-Hz, 90° Ricker wavelet, and the intrinsic attenuation of the medium is made negligible by setting $1/Q_i = 10^{-6}$.

The signal spectrum $S(f)$ is extracted from the maximum amplitude coefficients for each frequency in the spectrogram. This allows for dispersion, because not all frequencies must have the same maximum-amplitude arrival time. The reference-signal spectrum $S_0(f)$ is obtained from an identical synthetic setup using a homogeneous medium, which eliminates potential problems resulting from geometric spreading and numerical dispersion (van der Baan, 2001). Finally, the estimated attenuation profiles are determined using equation 2, and the $1/Q_{sc}$ is inspected using the Aki and Richards (2002) definition (equation 3). The theoretical frequency-dependent $1/Q_{sc}$ caused by scattering is obtained using equations 3 and 18.

Table 1. Measured and modeled parameters for a medium with random velocity v_P fluctuations that exhibit an exponential autocorrelation. By assuming a constant density ρ, the relative standard deviation of the velocity σ_v is half of the relative standard deviation of incompressibility σ_κ. Note that although the scattering properties of models 2 and 3 are different, the apparent attenuation defined by equation 18 is the same for both.

	Well-log analysis	Blocked well log	Model 1	Model 2	Model 3	Model 4
Mean V_P (m/s)	2037	2067	2000	2000	4000	2000
Mean ρ (kg/m^3)	2104	2129	2100	2100	2100	2100
Relative σ_κ (%)	12.28	14.26	15	15	15	15
Relative σ_V (%)	6.14	7.13	7.5	7.5	7.5	7.5
Typical scale (m)	1.37	2	2	1	2	4

Results

Intermediate results are shown for only the first model from Table 1, as the remaining models show similar effects. A single realization of the velocity model and the signal transmitted through it are displayed in Figure 1. Here the time-domain effects of the multiple scattering are seen, where the direct arrival at 0.25 s is followed by coda energy from the multiples. In Figure 2, the spectrogram of the transmitted signal is shown using the four transforms outlined above. The major difference between the fixed-window transforms (Figure 2a and b) and the variable-window transforms (Figure 2c and d) is in the shape of the primary arrival in time-frequency space. This shape is relat-

ed directly to the transform window size, and for the variable-window transforms, the distinct wedge is evident, narrowing in time toward higher frequencies.

What is apparent also from Figure 2 is that the coda energy is not just separated from the direct arrival in time, but in frequency as well. This is indicated by the lower amplitude energy centered between 50 and 150 Hz, which follows the primary arrival at 0.26 s. More significant is that in the variable-window transforms, the coda energy above 100 Hz shows less interference with the primary energy.

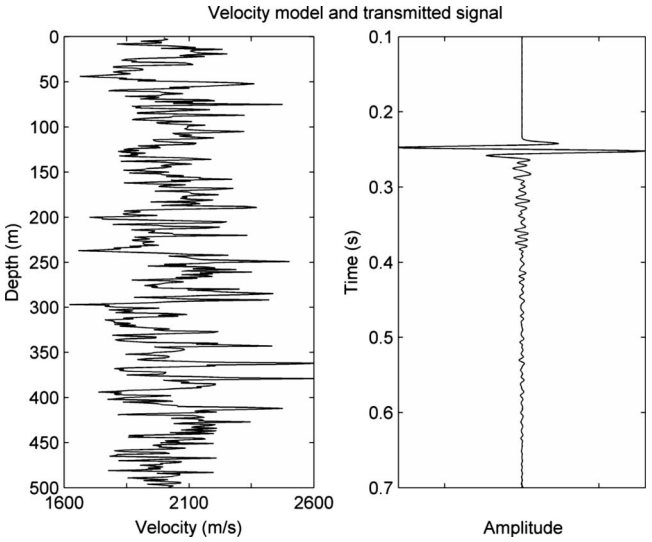

Figure 1. A single realization of randomly fluctuating velocities defined by the parameters of model 1 (Table 1), and the seismic signal transmitted through it. The coda follows the primary arrival after 0.26 s. Relative amplitudes are shown.

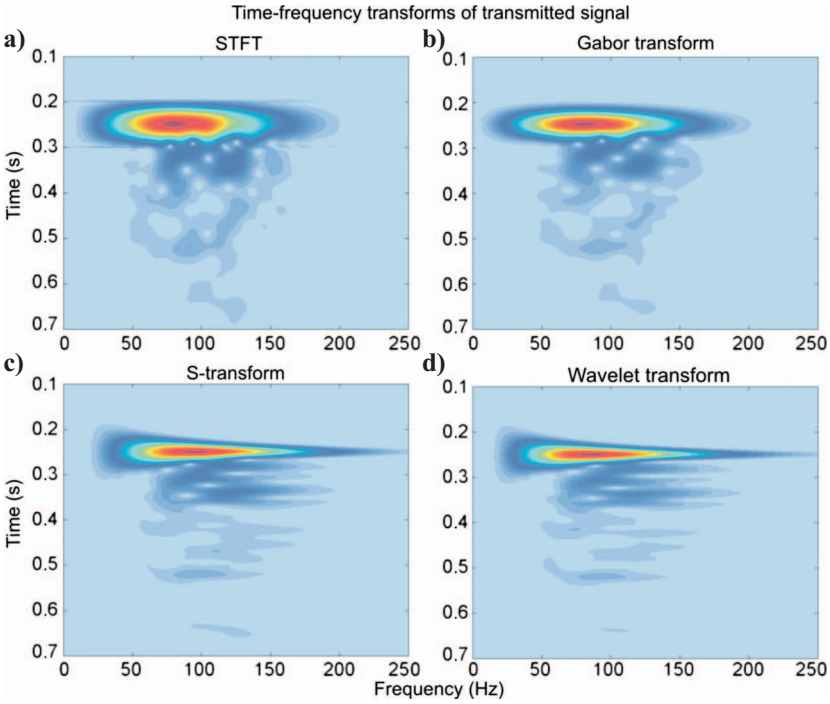

Figure 2. Time-frequency plots of the signal shown in Figure 1. The highest amplitudes (red colors) are for the primary arrival, whose shape in the time-frequency domain is determined by the transform window functions. The interference effects between the primary arrival and coda can be seen as "holes" in the spectrum. (a) STFT, (b) Gabor transform, (c) S-transform, and (d) wavelet transform. The frequency axis of the wavelet transform has been rescaled to a linear frequency display.

After extracting the maximum amplitude spectra from each transform, the respective $1/Q_{sc}$ functions are calculated for each realization, examples of which are shown in Figure 3a. The frequency-dependent curves fluctuate significantly about the theoretical predictions as a result of the finite number of layers in the model, and the interference of the coda that results from multiple scattering. To account for the finite layers, and to look at systematic deviations, we must take a look at the mean of the $1/Q_{sc}$ estimates from all realizations.

The mean of the estimated attenuation from each transform is shown in Figure 3b. The statistical fluctuations are reduced, and the main effects, which are visible, are fluctuations caused by coda interference. Below 10 Hz and above 200 Hz, large variations result because the measurements fall outside the significant bandwidth of the data. The deviations from the theoretical curves are similar for all of the transforms, with an improvement from the variable-window transforms for frequencies above 110 Hz and below 30 Hz.

More significantly, the uncertainty in the measurement of a single realization is shown by the standard deviation of the distribution of estimates, shown in Figure 3c. The standard deviation of the attenuation estimates is smaller for the variable-window transforms, with an exception of the frequencies between 30 and 55 Hz, where the results show no major differences. In this frequency range, the window lengths for all of the transforms are similar. The most significant improvements in the standard deviation are above 100 Hz. This suggests that individual amplitude spectra produced by the variable-window transforms are more precise, having a narrower statistical distribution. The analysis is repeated for models 2–4 from Table 1. Figure 4 shows the standard deviations for the $1/Q_{sc}$ estimates for these models, and again, the results show that the variable-window transforms have a lower variability than the fixed-window transforms, specifically at higher frequencies.

Reducing the size of the time window in the STFT and Gabor transform obtains similar high-frequency results to the variable-window transforms. The detriment of reducing the time window, however, is seen in Figure 5, which shows one realization of the $1/Q_{sc}$ estimate from the STFT with different-length time windows. Although the fluctuations at high frequencies are reduced, the minimum frequency for which $1/Q$ can be measured properly also increases. This is seen by the short-window curves, which have large deviations at the low end of the spectrum.

REFLECTION AND CONSTANT Q ATTENUATION

Objective

For the second experiment, we measure the effective attenuation from a synthetic zero-offset

surface seismic geometry. Because there is no simple analog to wave localization theory for reflection data, we use a different test to demonstrate the effects shown in the transmission experiment. We create a 1D model, which experiences a uniform constant-Q intrinsic attenuation in addition to scattering losses.

Although frequency-dependent multiple scattering is present in all data, it is common to assume a frequency-independent effective $1/Q_e$ within the seismic bandwidth (Sams et al., 1997). This is a worthwhile first approximation as long as the frequency-independent intrinsic attenuation is large compared with the apparent scattering attenuation. The assumption also implies that an effective $1/Q_e$ estimate from a linear regression of the natural log spectral ratio should be the same regardless of the bandwidth chosen. In fact, spectral fluctuations, which result in part from multiple scattering, cause the linear regression to be highly dependent on the choice of bandwidth. This is true also for regressions that allow for a nonlinear relationship between the natural log spectral ratio and frequency (Reid et al., 2001). In the second experiment, we test the ability of the time-frequency transforms to produce $1/Q_e$ estimates that are robust with respect to the bandwidth used in the regression.

Test setup

We create first a 1D medium from the blocked velocity and density logs of the well data used in the transmission test. We impose a uniform intrinsic attenuation with $1/Q_i = 0.020$, and produce zero-offset reflection seismic data with a 70-Hz, 90° Ricker source wavelet (Figure 6). In Figure 6, two reflectors are indicated that correspond to large velocity and density changes in the model. We extract the spectra from these two times and calculate the effective attenuation from a linear regression of their natural log spectral ratios, using

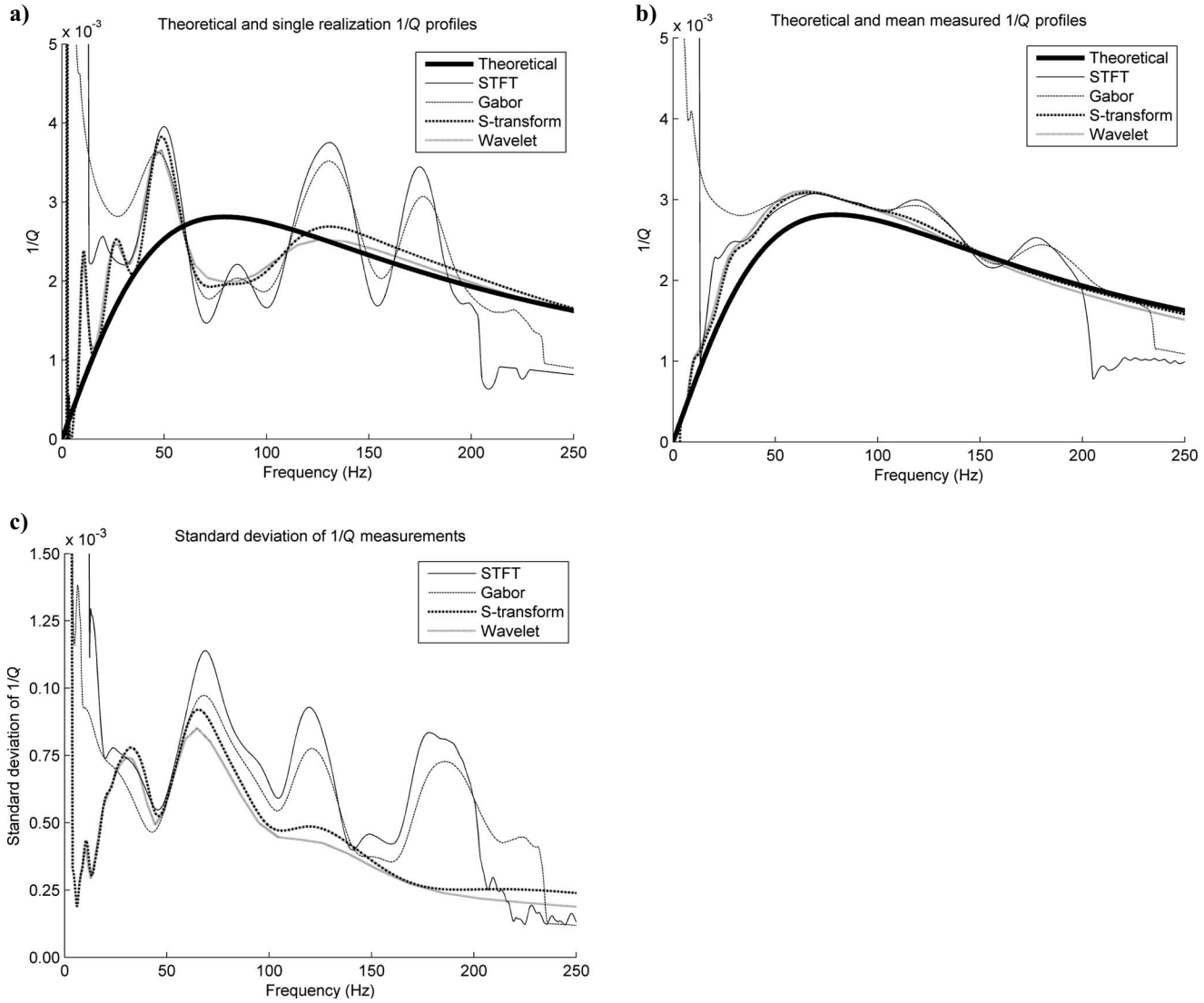

Figure 3. The theoretical and estimated $1/Q_{sc}$ for (a) a single realization of the transmitted primary signal through the randomly fluctuating velocity model, and (b) the mean of 20 realizations. The mean curve reduces statistical fluctuations for better analysis of the systematic deviations. The estimated frequency-dependent $1/Q_{sc}$ fluctuates about the theoretical curve resulting from effects of spectral interference with the coda energy. The values are similar for all transforms, with a slight improvement from the variable-window transforms below 30 Hz and above 110 Hz. (c) Standard deviation of the 20 realizations of estimated $1/Q_{sc}$ showing the frequency-dependent variability of the estimates. The variable-window transforms show improvement below 25 Hz and above 90 Hz, indicating a more precise estimate.

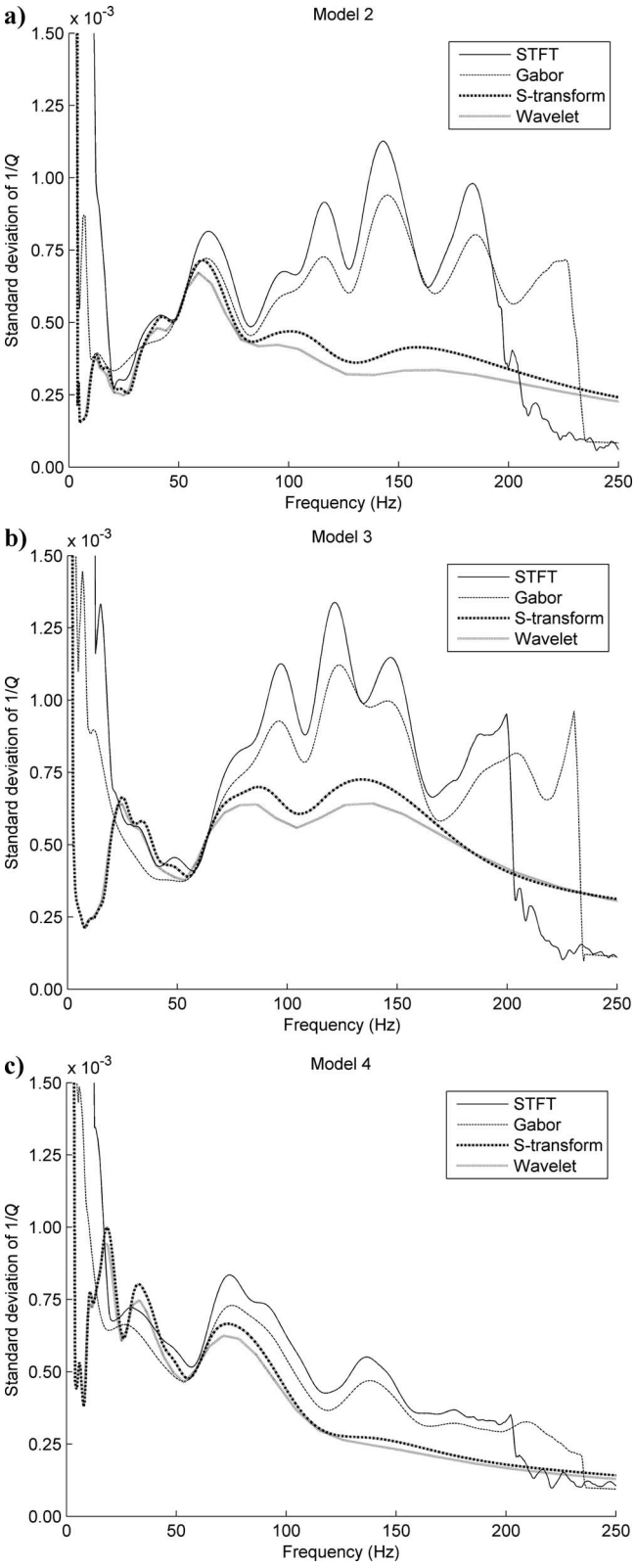

Figure 4. (a-c) Standard deviations of estimated $1/Q_{sc}$ for models 2-4, respectively. The improvement in the standard deviation for the variable-window transforms agrees with the data shown in Figure 3c.

equation 2. Because initial and final spectra, $S_0(f)$ and $S(f)$, are subject to scattering and interference, spectral notching exists in both, contrary to the transmission test in which only the final spectrum $S(f)$ was affected. We repeat the regression for different bandwidths, varying the lower frequency from 0 through 110 Hz, and the upper frequency between 90 and 250 Hz.

Although not strictly accurate, we use equations 3 and 18 to provide a rough estimate of the scattering attenuation for the medium.

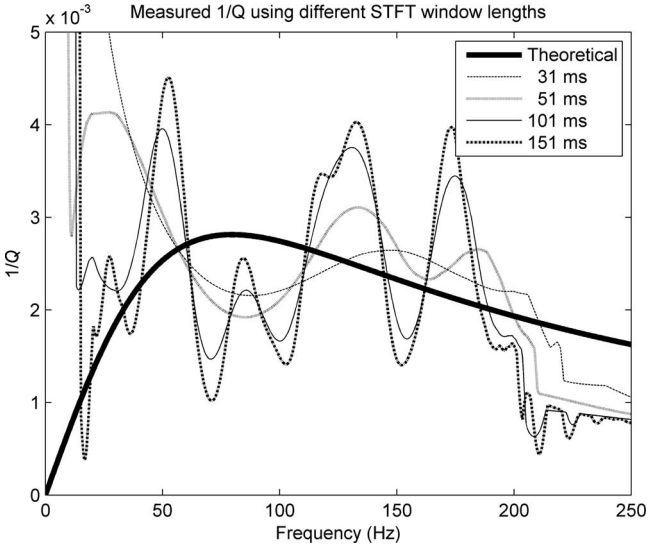

Figure 5. Theoretical and estimated $1/Q_{sc}$ for the single realization of the fluctuating velocity model shown in Figure 1 using different window lengths of the STFT. Whereas the smaller windows reduce fluctuations at higher frequencies, the low frequencies are not measured properly.

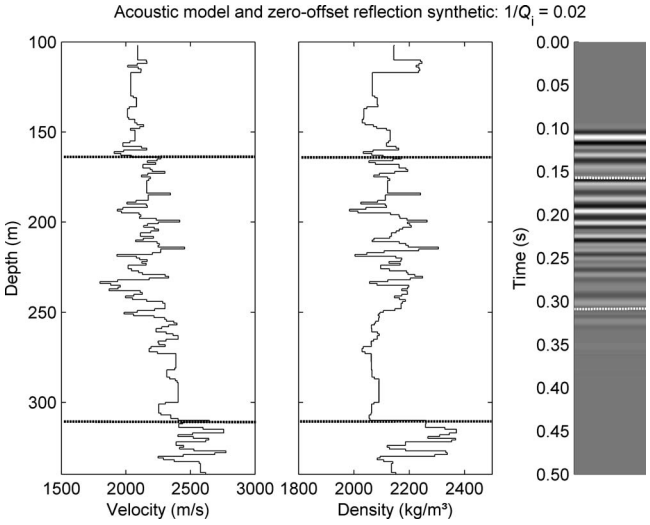

Figure 6. From left to right, the blocked P-wave velocity and density logs, and the resulting zero-offset reflection synthetic (normal polarity with black peaks). The dashed lines at 164 and 310 m (159 ms and 309 ms) indicate two major impedance changes whose reflections are used in the $1/Q$ analysis. The logs have been blocked with an average block size of 2 m.

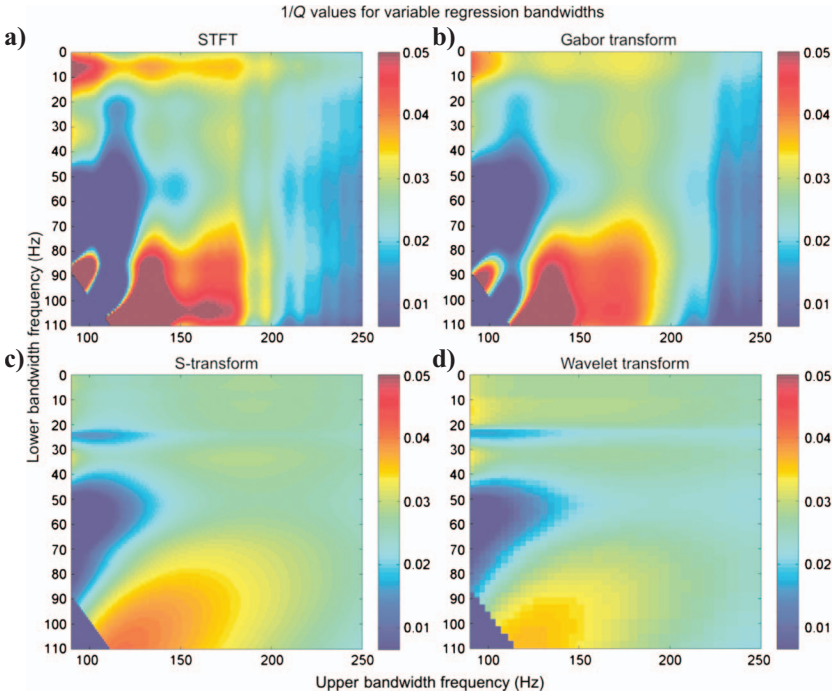

Figure 7. The $1/Q_e$ values estimated for a range of lower and upper bandwidth frequencies using the spectra derived from the different transforms. (a) STFT: The area of stability near the input $1/Q_i = 0.020$ is seen for lower frequencies between 15 and 65 Hz, and upper ones between 125 and 200 Hz. (b) The Gabor transform has the same stable zone as the STFT. (c) The S-transform extends the stable zone to 0 through 70 Hz for the lower frequencies, and to 125 through 250 Hz for the upper ones. (d) Results for the wavelet transform show similar results to the S-transform. The axes of the wavelet transform have been rescaled to a linear frequency display.

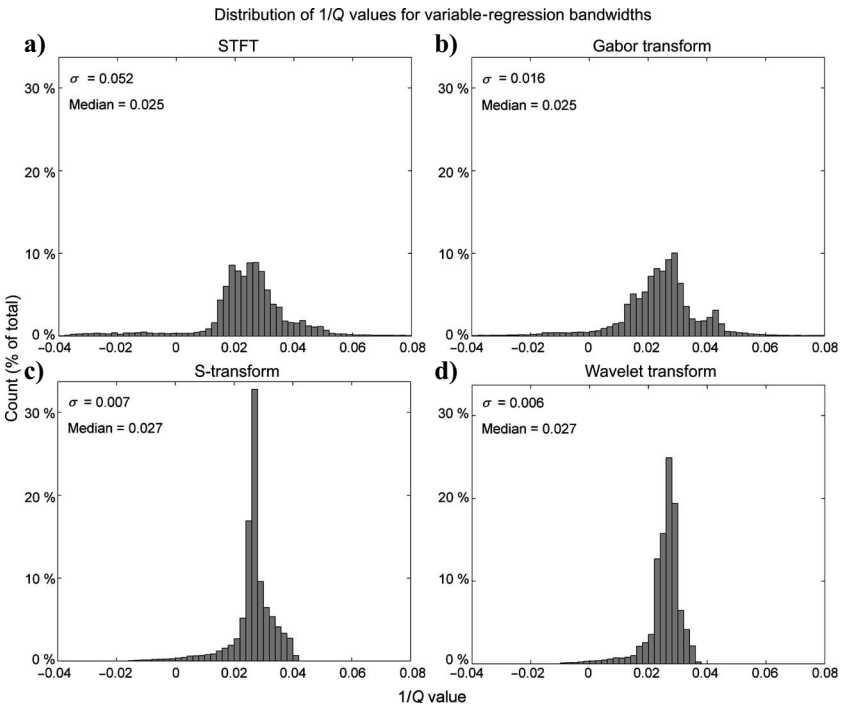

Figure 8. Histograms of the $1/Q_e$ estimates shown in Figure 7. (a) STFT, (b) Gabor transform, (c) S-transform, (d) wavelet transform; (a) and (b) show a broader spread in values, with more outlying values than for (c) and (d). The standard deviations and median values of the distributions are indicated, showing that variable-window transforms are less sensitive to the choice of regression bandwidth.

Using the parameters calculated for the blocked well log in Table 1, the maximum $1/Q_{sc}$ for the medium occurs at 82 Hz and has a value of $1/Q_{sc} = 0.003$. Although not exact, this estimation shows that the apparent attenuation is an order of magnitude smaller than the imposed intrinsic attenuation for this model, consistent with observations made by Sams et al. (1997). The effective $1/Q_e$ for the medium therefore should be approximately 0.023 (equation 5).

Results

For each discrete bandwidth choice, a $1/Q_e$ value is calculated and plotted in Figure 7. In this plot, large areas of the same color indicate that the $1/Q_e$ estimate is stable with the choice of bandwidth. Ideally, this stable value should correspond to the effective attenuation, a combination of the input intrinsic attenuation and apparent attenuation from multiple scattering. Areas at the extreme ends of the color scale indicate that the regression result is dominated by peaks and notches in the natural log spectral ratio.

Figure 7a and b, for the fixed-window transforms, are similar in appearance. The most stable region that corresponds to the approximate $1/Q_e$ is found roughly in the center of the plot, between 15 and 65 Hz on the vertical axis and 125 Hz through 200 Hz on the horizontal axis. The plots corresponding to the variable-window transforms, Figure 7c and d, extend this stable area back to nearly 0 Hz on the vertical axis, and out through 250 Hz on the horizontal axis. In practice, the extent of the stable bandwidths also would be reduced by the signal-to-noise ratio.

Again, the benefits of reduced fluctuations from the variable-window transforms are seen on the histograms of the $1/Q_e$ data in Figure 8. The histograms for the S-transform and wavelet transform show a more peaked distribution ($\sigma_S = 0.007$, $\sigma_W = 0.006$) compared with those of the STFT and Gabor transform ($\sigma_F = 0.052$, $\sigma_G = 0.016$). This indicates that the estimated $1/Q_e$ values for these transforms are less susceptible to the choice of regression bandwidth because they more closely match the expectation of a single value that is independent of bandwidth. Conversely, the histograms of the STFT and Gabor transform indicate a larger variability in results, and they include $1/Q_e$ values farther from the central peak.

It should be noted also that the median value of the distributions is $1/Q_e = 0.025$ for the fixed-window transforms and $1/Q_e = 0.027$ for the variable-window transforms. The median values are higher than the intrinsic $1/Q_i = 0.020$ because of the apparent attenuation effects. The difference between the effective and intrinsic values is of the same order of magnitude as the approxi-

mation calculated above ($1/Q_{sc} = 0.003$). The difference in the median values for the fixed- and variable-window transforms could be the result of differences in the systematic bias for a single realization, the bias introduced by the variable-window transform being smaller (Figure 3a).

SURFACE SEISMIC ANALYSIS

Our final analysis is the measurement of an average $1/Q_e$ for a surface seismic CMP gather from the Alberta oil sands in Canada. The data have a shallow zone of interest (two-way traveltime <400 ms) and image an unconsolidated sandstone containing very heavy oil. This unconsolidated sandstone is overlain by alternating sandstone and siltstone layers. As with the synthetic reflection experiment, there is no theoretically expected value for the attenuation in these data. We look therefore at the robustness of the $1/Q_e$ estimate with the choice of bandwidth, in addition to the statistics of how well the attenuation measurements match the expected offset-dependent behavior.

Q-versus-offset method

Dasgupta and Clark (1998) describe a method for measuring attenuation from prestack surface seismic data. The first step involves calculating the natural log spectral ratio slopes A as functions of frequency for a reflection at each offset relative to a reference wavelet (equation 4). Because these slopes are proportional to traveltime, a second regression then can be performed to estimate the value of A at zero offset. The final step is to convert this value to a zero-offset $1/Q_e$ estimate.

Whereas Dasgupta and Clark (1998) use a small-spread approximation and perform the second regression versus offset squared, Carter (2003) points out that this assumption is unnecessary if the measured traveltime is used directly. In this case, we perform a linear regression of the form

$$A = -\frac{\pi}{Q}\Delta t, \tag{20}$$

where Δt is the traveltime difference between the reflection and reference wavelet. The Q-versus-offset (QVO) method assumes that there is a homogeneous and isotropic overburden with a horizontal reflector. Although this never is perfectly the case, the geology of this particular data set is a good approximation, and the method still provides useful insight into the attenuation behavior of the medium.

Test setup

The data that we analyze consist of a 3×3 grid of CMP gathers extracted from a 3D survey. The survey was acquired using single explosive sources and single multicomponent digital receivers. The source and receiver spacing were 20 m, resulting in a 10- $\times$ 10-m bin size. We apply minimal processing to the seismic data so as to avoid introducing lateral and temporal changes to the spectrum. Refraction and residual statics are applied, along with trace edits and a trapezoidal (10–20–120–180 Hz) band-pass filter. To improve the signal-to-noise ratio, the CMPs are formed into a single stacked supergather. The offset range is restricted to 416 m, which provides 40 traces of data to a maximum offset-to-depth ratio of approximately 1.2. The final CMP supergather is shown in Figure 9.

The reflection that we analyze has a zero-offset time of 324 ms, which is near the base of the zone of interest. Rather than use NMO-corrected data, we calculate the hyperbolic traveltimes using the stacking velocity field. Then we shift the center of the analysis along this curve, thereby avoiding the need to apply an NMO stretch correction to the spectra. For a reference wavelet, we use the direct arrival from a near-offset trace. Because the data are acquired with point sources and receivers, there are no directivity effects on the spectrum to consider (Hustedt and Clark, 1999).

Results

We test first the stability of the natural log spectral ratio slopes A with the choice of regression bandwidth. The bandwidth-dependent slopes of a near (159-m) and far (350-m) offset are shown in Figure 10, in which for consistency, the data have been scaled to show $1/Q_e$. This analysis shows results that are consistent with the synthetic experiments. Specifically, for the far-offset example, the variable-window transforms significantly extend the lower bandwidth frequency that produces a uniform $1/Q_e$ estimate. For the near-offset case, the fixed-window transforms show an abrupt change in $1/Q_e$ as the lower frequency is increased, whereas the variable-window transforms have a much more gradual change.

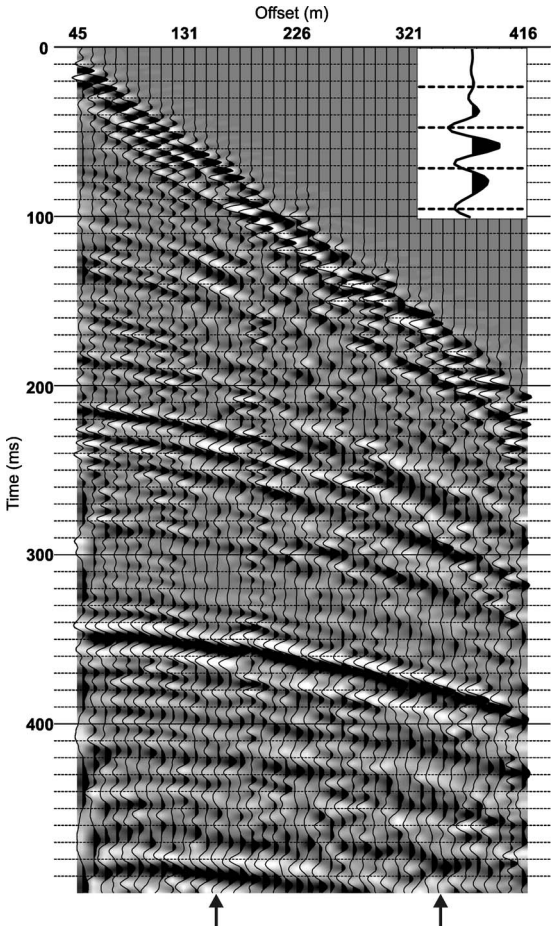

Figure 9. CMP supergather used in the QVO analysis. An enlargement of the reference wavelet is shown, and the offsets analyzed in Figure 10 are indicated by arrows. A 100-ms automatic gain control and a top mute have been applied for display purposes.

Because attenuation increases with traveltime, the relationship between A and Δt is expected to be linear with a negative slope. In reality, the measurements fluctuate about this trend because of noise in the data, spectral interference, and apparent attenuation effects. To quantify how closely the measurements of A and Δt follow the theoretical behavior, we calculate the correlation coefficient. Given two variables, the correlation coefficient measures the degree to which they are related linearly. The values range between minus one and one corresponding to a perfect negative and positive correlation, respectively, whereas a value of zero indicates uncorrelated data (Taylor, 1997). Figure 11 shows the correlation coefficients derived for the four transforms, and these data show that A and Δt have a stronger correlation when measured by the variable-window transforms. These transforms also extend the bandwidth range in which this expected behavior is observed.

Finally, Figure 12 shows the bandwidth dependency of the zero-offset $1/Q_e$ estimate from the A versus Δt regression. This result clearly shows that the variable-window transforms produce $1/Q_e$ estimates that are more robust than their fixed-window counterparts. Furthermore, the $1/Q_e$ values obtained are consistent with the type of geology investigated. Macrides and Kanasewich (1987), for example, use a crosswell experiment to find a value of $1/Q_e = 0.03$ in unconsolidated heavy-oil reservoirs. Although this does not account for attenuation in the overburden, the findings are consistent with our measurements.

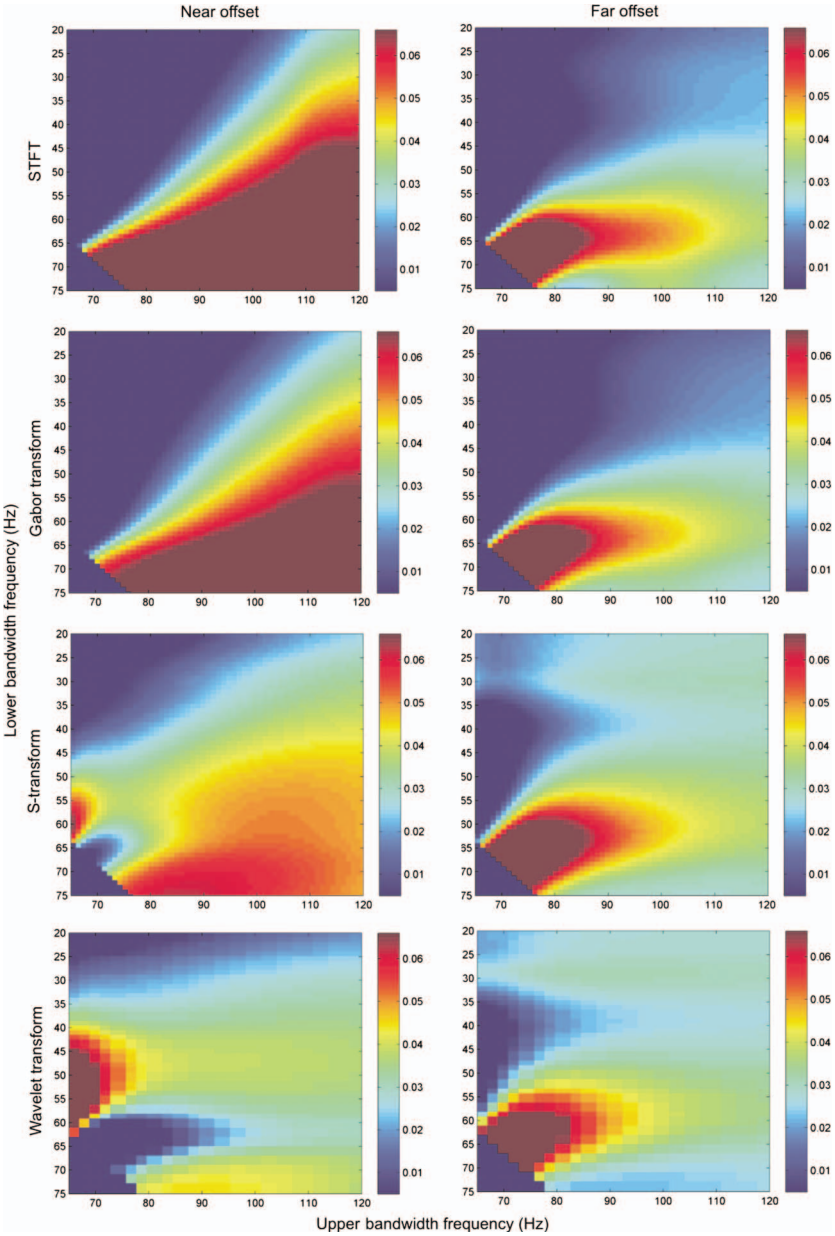

Figure 10. The $1/Q_e$ values for the near offset trace (left side) and far offset trace (right side), estimated over a range of bandwidths. At both trace offsets, the variable-window transforms (lower half) increase the number of bandwidth choices that produce a stable $1/Q_e$ estimate.

DISCUSSION

A single estimate of frequency-dependent $1/Q_{sc}$ for a transmitted pulse is more accurate and has less uncertainty when made with a time-frequency transform that uses a variable-length time window instead of a fixed-length time window. This is shown by the statistical properties displayed in Figure 3. Similarly, when estimating a frequency-independent $1/Q_e$ for both a synthetic and a real data reflection experiment, the variable-window transforms produce results that are more robust with respect to the choice of regression bandwidth.

These observations arise because the variable-window transforms reduce the extent of the spectral fluctuations for two reasons. First, at high frequencies, at which typically more energy is scattered to the coda, there is an increase in the degree of nonstationarity in the data. The variable time windows use shorter time windows to analyze the high frequencies, so that the primary arrival is better isolated from the coda. This can be seen in Figure 2, in which at higher frequencies, the spectrum of the primary arrival is more distinct from the spectrum of the coda for variable-window transforms. Although the variable windows isolate high frequencies as noted, they also include a larger portion of coda at lower frequencies. This is not detrimental, because (1) only small amounts of low-frequency energy are in the coda as a result of the nature of the scattering and (2) in a given time window, the variability of attenuation for lower frequencies is less than that for higher frequencies because of the reduced number of wavelengths present.

The second reason behind the reduction of fluctuations also is related to window size. Because of the Gabor uncertainty principle (Hall, 2006), as the time window becomes shorter, the effective frequency window increases in size. This means that there is an increased spectral averaging for the shorter windows, and any rapid fluctuations in the spectrum are smoothed out. Of course, the converse is true also, namely, that

there is higher spectral resolution for the longer time windows at low frequencies.

Although it is possible to isolate the coda from the signal by using a shorter window length for the fixed-window transforms, this is not an ideal solution for broadband data. Figure 5 shows that the fluctuations about the theoretical value are reduced at higher frequencies, but the minimum frequency that can be measured properly increases also. This makes short windows detrimental for data consisting of a large frequency range. The variable-window transforms do not face this problem, as they maintain a window length that is proportional to the period being analyzed.

The small differences between the results of the S-transform and wavelet transform demonstrate why it is more significant to compare classes of transforms, rather than the individual transforms themselves. Small changes in the transform parameters or in the data being analyzed can create situations in which either variable-window transform will show a small benefit over the other. Nevertheless, we prefer the S-transform over the wavelet transform because it produc-

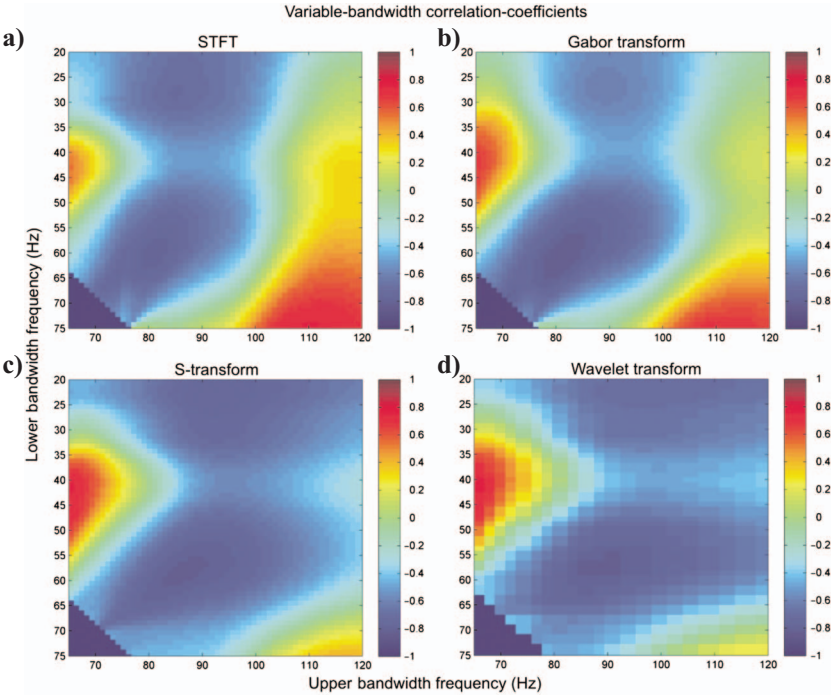

Figure 11. Correlation coefficient plots between A and Δt for the (a) STFT, (b) Gabor transform, (c) S-transform, and (d) wavelet transform. The theoretical relationship results in a value of -1, and (c) and (d) more closely approach this value over a larger choice of bandwidths.

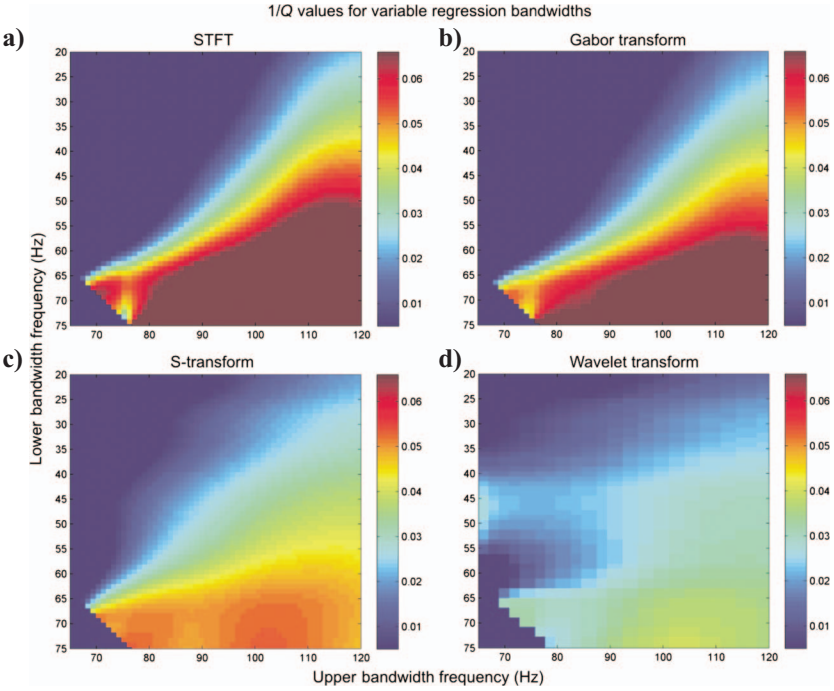

Figure 12. The final $1/Q_e$ estimates from the QVO method. As with previous results, estimates of the (a) STFT and (b) Gabor transform are less stable than the (c) S-transform and (d) wavelet-transform measurements.

es spectral estimates as a function of frequency rather than scale, and because it preserves the time reference of the data's phase information (Stockwell et al., 1996).

CONCLUSIONS

We have conducted two experiments to test what difference the choice of time-frequency transform makes when measuring seismic attenuation. We investigated two classes of transforms, those with fixed time windows and those with systematically varying time windows, in the context of measuring a frequency-dependent $1/Q_{sc}$ caused by multiple scattering, and a frequency-independent effective $1/Q_e$ from a linear regression of natural log spectral ratios versus frequency.

We have shown that the time-frequency transform used to calculate the spectrum of a transmitted wave influences the precision and accuracy of attenuation estimates. The S-transform and continuous wavelet transform decrease the variability of the attenuation estimate, specifically at the high and low ends of the spectrum. For higher frequencies, the variability is reduced for two reasons: (1) the primary arrival is isolated from the coda by the shorter time windows used for higher frequencies; and (2) the shorter window results in spectral averaging, thereby reducing the influence of spectral fluctuations such as notches and peaks. At the low-frequency end, improvements are the results of proper amplitude determination by maintaining an adequate signal sample for each period.

Variable-window transforms also improve the robustness of a frequency-independent effective $1/Q_e$ estimate obtained using a linear regression of natural log spectral ratios versus frequency. This offers more flexibility in the choice of bandwidth used for the regression. The increased robustness is seen in the analysis of a real data set, in which attenuation measurements across multiple offsets more closely follow an expected linear behavior with traveltime when they are made with variable-window transforms instead of fixed-window transforms. These measurements led to a determination of $1/Q_e$ that is consistent with previously measured values. We therefore find that variable-window transforms, such as the S-transform and wavelet transform, offer distinct benefits for seismic attenuation analysis, in cases when a nonstationary signal must be evaluated.

ACKNOWLEDGMENTS

Funding for this research was kindly provided by Nexen Inc. We also thank Nexen Inc. and OPTI Canada Inc. for providing the well-log and seismic data for our analysis. In addition, discussions with Andrew Carter on attenuation, and input from Matt Hall and an anonymous reviewer, are greatly appreciated.

REFERENCES

Aki, K., and P. G. Richards, 2002, Quantitative seismology, 2nd ed.: University Science Books.
Bracewell, R., 1978, The Fourier transform and its applications, 2nd ed.: McGraw-Hill Inc.
Carmona, R., W. Hwang, and B. Torresani, 1998, Practical time-frequency analysis: Gabor and wavelet transforms with an implementation in S: Academic Press.
Carter, A. J., 2003, Seismic wave attenuation from surface seismic reflection surveys — An exploration tool?: Ph.D. thesis, University of Leeds.
Castagna, J. P., and S. Sun, 2006, Comparison of spectral decomposition methods: First Break, **24**, 75–79.
Chakraborty, A., and D. Okaya, 1995, Frequency-time decomposition of seismic data using wavelet-based methods: Geophysics, **60**, 1906–1916.
Clark, R. A., A. J. Carter, P. C. Nevill, and P. M. Benson, 2001, Attenuation measurements from surface seismic data — Azimuthal variation and time-lapse case studies: 63rd Conference and Technical Exhibition, EAGE, Expanded Abstracts, L-28.
Dasgupta, R., and R. A. Clark, 1998, Estimation of Q from surface seismic reflection data: Geophysics, **63**, 2120–2128.
Daubechies, I., 1992, Ten lectures on wavelets: Society for Industrial and Applied Mathematics.
Dietrich, M., 1988, Modeling of marine seismic profiles in the t-x and τ-p domains: Geophysics, **53**, 453–465.
Dvorkin, J., and A. Nur, 1993, Dynamic poroelasticity — A unified model with the squirt and the Biot mechanisms: Geophysics, **58**, 524–533.
Hall, M., 2006, Resolution and uncertainty in spectral decomposition: First Break, **24**, 43–47.
Harris, F. J., 1978, Use of windows for harmonic analysis with discrete Fourier transform: Proceedings of the IEEE, **66**, 51–83.
Hauge, P. S., 1981, Measurements of attenuation from vertical seismic profiles: Geophysics, **46**, 1548–1558.
Hustedt, B., and R. A. Clark, 1999, Source/receiver array directivity effects on marine seismic attenuation measurements: Geophysical Prospecting, **47**, 1105–1119.
Johnston, D. H., M. N. Toksoz, and A. Timur, 1979, Attenuation of seismic waves in dry and saturated rocks: II — Mechanisms: Geophysics, **44**, 691–711.
Kaderali, A., M. Jones, and J. Howlett, 2007, White Rose seismic with well data constraints: A case history: The Leading Edge, **26**, 742–754.
Li, H., W. Zhao, H. Cao, F. Yao, and L. Shao, 2006, Measures of scale based on the wavelet scalogram with applications to seismic attenuation: Geophysics, **71**, no. 5, V111–V118.
Luh, P. C., 1993, Wavelet attenuation and bright-spot detection, *in* J. P. Castagna and M. M. Backus, eds., Offset-dependent reflectivity: Theory and practice of AVO analysis: Investigations in Geophysics, 8, 190–198.
Macrides, C. G., and E. R. Kanasewich, 1987, Seismic attenuation and Poisson's ratios in oil sands from crosshole measurements: Journal of the Canadian Society of Exploration Geophysicists, **23**, 46–55.
Mallat, S. G., and Z. F. Zhang, 1993, Matching pursuits with time-frequency dictionaries: IEEE Transactions on Signal Processing, **41**, 3397–3415.
Maultzsch, S., M. Chapman, E. Liu, and X.-Y. Li, 2007, Modelling and analysis of attenuation anisotropy in multi-azimuth VSP data from the Clair field: Geophysical Prospecting, **55**, 627–642.
O'Doherty, R. F., and N. A. Anstey, 1971, Reflections on amplitudes: Geophysical Prospecting, **19**, 430–458.
Reid, F. J. L., P. H. Nguyen, C. MacBeth, R. A. Clark, and I. Magnus, 2001, Q estimates from north sea VSPs: 71st Annual International Meeting, SEG, Expanded Abstracts, 440–443.
Rioul, O., and M. Vetterli, 1991, Wavelets and signal processing: IEEE Signal Processing Magazine, 1991, 14–38.
Sams, M. S., J. P. Neep, M. H. Worthington, and M. S. King, 1997, The measurement of velocity dispersion and frequency-dependent intrinsic attenuation in sedimentary rocks: Geophysics, **62**, 1456–1464.
Schoenberger, M., and F. K. Levin, 1974, Apparent attenuation due to intrabed multiples: Geophysics, **39**, 278–291.
———, 1978, Apparent attenuation due to intrabed multiples, II: Geophysics, **43**, 730–737.
Shapiro, S. A., and H. Zien, 1993, The O'Doherty-Anstey formula and localization of seismic waves: Geophysics, **58**, 736–740.
Sinha, S., P. S. Routh, P. D. Anno, and J. P. Castagna, 2005, Spectral decomposition of seismic data with continuous-wavelet transform: Geophysics, **70**, no. 6, P19–P25.
Spencer, T. W., C. M. Edwards, and J. R. Sonnad, 1977, Seismic-wave attenuation in nonresolvable cyclic stratification: Geophysics, **42**, 939–949.
Spencer, T. W., J. R. Sonnad, and T. M. Butler, 1982, Seismic Q — Stratigraphy or dissipation: Geophysics, **47**, 16–24.
Stockwell, R. G., L. Mansinha, and R. P. Lowe, 1996, Localization of the complex spectrum: The S transform: IEEE Transactions on Signal Processing, **44**, 998–1001.
Tai, S., D. Han, and J. P. Castagna, 2006, Attenuation estimation with continuous wavelet transforms: 76th Annual International Meeting, SEG, Expanded Abstracts, 1933–1937.
Taylor, J. R., 1997, An introduction to error analysis: The study of uncertainties in physical measurements, 2nd ed.: University Science Books.
Tonn, R., 1991, The determination of the seismic quality factor Q from VSP data — A comparison of different computational methods: Geophysical Prospecting, **39**, 1–27.
Toverud, T., and B. Ursin, 2005, Comparison of seismic attenuation models using zero-offset vertical seismic profiling (VSP) data: Geophysics, **70**, no. 2, F17–F25.
van der Baan, M., 2001, Acoustic wave propagation in one-dimensional random media: The wave localization approach: Geophysical Journal International, **145**, 631–646.

van der Baan, M., J. Wookey, and D. Smit, 2007, Stratigraphic filtering and source penetration depth: Geophysical Prospecting, **55**, 679–684.
Wang, Y. H., 2002, A stable and efficient approach of inverse Q filtering: Geophysics, **67**, 657–663.
———, 2007, Seismic time-frequency spectral decomposition by matching pursuit: Geophysics, **72**, no. 1, V13–V20.
Winkler, K. W., and A. Nur, 1982, Seismic attenuation — Effects of pore fluids and frictional sliding: Geophysics, **47**, 1–15.